

Nuclear Multifragmentation: Basic Concepts

G. CHAUDHURI^{a,*}, S. MALLIK^{a,†}, S. DAS GUPTA^{b,‡}

^aPhysics Group, Variable Energy Cyclotron Centre, 1/AF Bidhannagar, Kolkata 700064, India

^bPhysics Department, McGill University, Montréal, Canada H3A 2T8

Abstract. We present a brief overview of nuclear multifragmentation reaction. Basic formalism of canonical thermodynamical model based on equilibrium statistical mechanics is described. This model is used to calculate basic observables of nuclear multifragmentation like mass distribution, fragment multiplicity, isotopic distribution and isoscaling. Extension of canonical thermodynamical model to a projectile fragmentation model is outlined. Application of the projectile fragmentation model for calculating average number of intermediate mass fragments and the average size of largest cluster at different Z_{bound} , differential charge distribution and cross-section of neutron rich nuclei of different projectile fragmentation reactions at different energies are described. Application of nuclear multifragmentation reaction in basic research as well as in other domains is outlined.

Keywords. Multifragmentation, canonical thermodynamical model, projectile fragmentation

PACS Nos. 25.70.Mn, 25.70.Pq

1. Introduction

The study of nuclear multifragmentation [1–6] is an important technique for understanding the reaction mechanism in heavy ion collisions at intermediate and high energies. Due to collision of projectile and target nuclei, an excited nuclear system is formed. If its excitation energy is greater than a few MeV/nucleon, then it breaks into many nuclear fragments of different masses. This is known as nuclear multifragmentation. Here 'multi' indicates 'more than two'. Generally in nuclear fission process the compound nucleus breaks into two fission fragments. Therefore multifragmentation can be considered as the higher energy version of fission. Usually in nuclear multifragmentation reactions, required energy of the projectile beam produced from particle accelerator varies from few MeV/nucleon to few GeV/nucleon. The time scales involved in nuclear multifragmentation reaction are at most of the order of several hundred fm/c ($1\text{fm}/c=3.33\times 10^{-24}$ sec).

Different theoretical models have been developed for throwing light on the nuclear multifragmentation reaction and for explaining the relevant experimental data. The theoretical models can be classified into two main categories: (i) Dynamical models (Boltzmann-Uehling-Uhlenbeck (BUU) model [1], Antisymmetrised Molecular Dynamics (AMD) model [2], Isospin dependent quantum molecular dynamics (IQMD) model [3] etc.) and

*gargi@vecc.gov.in

†swagato@vecc.gov.in

‡dasgupta@hep.physics.mcgill.ca

(ii) Statistical models (Canonical Thermodynamical Model (CTM) [4], Statistical multifragmentation model (SMM) [5], microcanonical model [6] etc.). In the dynamical models time evolution of the nucleons of projectile and target nuclei are studied whereas the statistical model calculations are based on the available phase space. Compared to dynamical models, statistical models are computationally much less intensive and can successfully handle different kinds of experimental data. In this article the basic formalism of the Canonical Thermodynamical Model (CTM) and its application for calculating mass distribution, fragment multiplicity, isotopic distribution and isoscaling are described.

Presently projectile fragmentation reaction is an important area of research in order to study the properties of exotic nuclei. So CTM is extended to a model for describing the projectile fragmentation reaction. Different important observables of projectile fragmentation like intermediate mass fragments, largest cluster size, differential charge distribution etc are calculated from this model and compared with experimental data.

The paper is structured as follows. In section 2, we give a brief introduction of different statistical models where as the details of Canonical Thermodynamical Model is described in section 3 and its results are represented in section 4. The extension of CTM to a projectile fragmentation model is described in section 5 and some results of projectile fragmentation are explained in section 6. Few applications of multifragmentation are mentioned in section 7 and finally summary and conclusions are presented in section 8.

2. Statistical Models of Multifragmentation

Nuclear multifragmentation reactions are successfully described by statistical models based on equilibrium scenario of different excited fragments at freeze-out condition [4–6]. In statistical models, one assumes that depending upon the original beam energy, the disintegrating system may undergo an initial compression and then begins to decompress. As the density of the system decreases, higher density regions will develop into composites. As this collection of nucleons begins to move outward, rearrangements, mass transfers, nuclear coalescence and most physics will happen until the density decreases so much that the mean free paths for such processes become larger than the dimension of the system. This condition is termed as freeze-out [5].

The disintegration of excited nuclei can be studied by implementation of different statistical ensembles. Calculation by microcanonical ensemble is most realistic but very difficult to implement. Usually the grand canonical models are easily solved and they are more commonly used. In grand canonical models total mass or total charge fluctuation is allowed but physically it is not allowed in intermediate energy nuclear reactions. Statistical multifragmentation model of Copenhagen [5], the microcanonical models of Gross [6] and Randrup and Koonin [7] are commonly used. Canonical Thermodynamical Model (CTM) [4] was introduced later is easier to implement analytically and its main advantage is that one can eliminate the computationally intensive Monte Carlo procedures by using the recursive technique of Chase and Mekzian [8]. The results from the models based on different ensembles converge only under certain conditions for finite nuclei [9, 10].

3. Canonical thermodynamical model (CTM)

Assuming that a system with A_0 nucleons and Z_0 protons at temperature T , has expanded to a higher than normal volume, the partitioning into different composites can be calculated according to the rules of equilibrium statistical mechanics. In a canonical model, the partitioning is done such that all partitions have the correct A_0, Z_0 (equivalently N_0, Z_0).

The canonical partition function is given by

$$Q_{N_0, Z_0} = \sum \prod \frac{\omega_{I,J}^{n_{I,J}}}{n_{I,J}!} \quad (1)$$

Here the sum is over all possible channels of break-up (the number of such channels is enormous); $\omega_{I,J}$ is the partition function of one composite with neutron number I and proton number J respectively and $n_{I,J}$ is the number of this composite in the given channel. The one-body partition function $\omega_{I,J}$ is a product of two parts: one arising from the translational motion and another is the intrinsic partition function of the composite:

$$\omega_{I,J} = \frac{V}{h^3} (2\pi mT)^{3/2} A^{3/2} \times z_{I,J}(int) \quad (2)$$

Here V is the volume available for translational motion; V will be less than V_f , the volume to which the system has expanded at break up. We use $V = V_f - V_0$, where V_0 is the normal nuclear volume. For all calculations in section 4 we have considered $V_f = 6V_0$, which is obtained from experimental measurements and theoretical data fitting.

The average number of composites with I neutrons and J protons can be written as

$$\langle n_{I,J} \rangle = \omega_{I,J} \frac{Q_{N_0-I, Z_0-J}}{Q_{N_0, Z_0}} \quad (3)$$

There are two constraints: $N_0 = \sum I \times n_{I,J}$ and $Z_0 = \sum J \times n_{I,J}$. Substituting eq.(3) in these two constraint conditions, two recursion relations [8] can be obtained. Any one recursion relation can be used for calculating Q_{N_0, Z_0} . For example

$$Q_{N_0, Z_0} = \frac{1}{N_0} \sum_{I,J} I \omega_{I,J} Q_{N_0-I, Z_0-J} \quad (4)$$

We list now the properties of the composites used in this work. The proton and the neutron are fundamental building blocks thus $z_{1,0}(int) = z_{0,1}(int) = 2$ where 2 takes care of the spin degeneracy. For deuteron, triton, ${}^3\text{He}$ and ${}^4\text{He}$ we use $z_{I,J}(int) = (2s_{I,J} + 1) \exp(-\beta E_{I,J}(gr))$ where $\beta = 1/T$, $E_{I,J}(gr)$ is the ground state energy of the composite and $(2s_{I,J} + 1)$ is the experimental spin degeneracy of the ground state. Excited states for these very low mass nuclei are not included. For mass number $A = 5$ and greater we use the liquid-drop formula. For nuclei in isolation, this reads ($A = I + J$)

$$z_{I,J}(int) = \exp \frac{1}{T} [W_0 A - \sigma(T) A^{2/3} - \kappa \frac{J^2}{A^{1/3}} - C_s \frac{(I-J)^2}{A} + \frac{T^2 A}{\epsilon_0}] \quad (5)$$

The expression includes the volume energy, the temperature dependent surface energy, the Coulomb energy and the symmetry energy. The term $\frac{T^2 A}{\epsilon_0}$ represents contribution from excited states since the composites are at a non-zero temperature.

We also have to state which nuclei are included in computing Q_{N_0, Z_0} (eq.(4)). For I, J , we include a ridge along the line of stability. The liquid-drop formula above also gives neutron and proton drip lines and the results shown here include all nuclei within the boundaries. The long range Coulomb interaction between different composites is included by the Wigner-Seitz approximation[5].

4. Results from CTM

Important properties of nuclear multifragmentation like mass distribution, fragment multiplicity, isotopic distribution and isoscaling are studied theoretically by using canonical thermodynamical model (CTM).

4.1 Mass Distribution

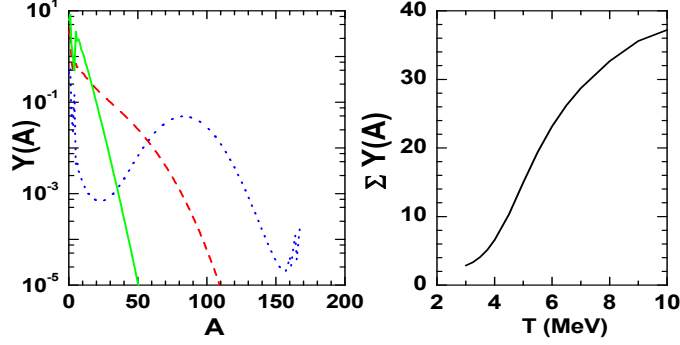


Figure 1. (Color online) Left panel: Theoretical mass distribution from $A_0 = 168$ and $Z_0 = 75$ system studied at $T=3$ MeV (blue dotted line), 5 MeV (red dashed line) and 7 MeV (green solid line). Right panel: Variation of total multiplicity with temperature.

Mass distribution of different fragments produced from the system of mass $A_0 = 168$ and charge $Z_0 = 75$ (it represents $^{112}\text{Sn} + ^{112}\text{Sn}$ central collisions after preequilibrium particle emission), is calculated at three different temperatures and is shown in left panel of Fig. 1. At $T=3.0$ MeV (lower excitation of compound nuclear system) fission is the dominating channel i.e. the multiplicity (total number of fragments) is about 2. But at $T=5$ MeV (moderate excitation), fission channel disappears and multi-fragmentation (breaking into large number of fragments) is the dominant process with a large number of intermediate mass fragments being formed. With further increase of temperature from 5 MeV to 7 MeV (very high excitation) the system mainly breaks into a larger number of smaller mass fragments. The variation of total fragment multiplicity with temperature is shown in the right panel of Fig. 1.

4.2 Isotopic Distribution

Isotopic distribution of $Z = 8$ and 14 fragments produced by multifragmentation of $A_0 = 168$ and $Z_0 = 75$ at two different temperatures $T = 5$ and 7 MeV are shown in Fig. 2(a) and 2(b). With the increase of temperature the isotopic distributions become wider. Multiplicities of different isotopes having $Z = 8$ and 14 produced from two different sources of charge $Z_0 = 75$ and masses $A_0 = 168$, $A_0 = 186$ is plotted in Fig. 2(c) and 2(d). From the isotopic distributions it is clear that the production of neutron rich fragments are more from the neutron rich source $Z_0 = 75$, $A_0 = 186$ compared to the other less neutron-rich $Z_0 = 75$, $A_0 = 168$.

4.3 Isoscaling

Isoscaling [11, 12] is an important property for studying the symmetry energy in intermediate energy nuclear reactions. It is observed both theoretically and experimentally that the ratio of yields $R_{21} = Y_2(N, Z)/Y_1(N, Z)$ from two reactions 1 and 2 having different isospin asymmetry (2 is more neutron rich than 1) exhibit an exponential relationship as a function of neutron(N) and proton(Z) number i.e.

$$R_{21} = Y_2(N, Z)/Y_1(N, Z) = C \exp(\alpha N + \beta Z) \quad (6)$$

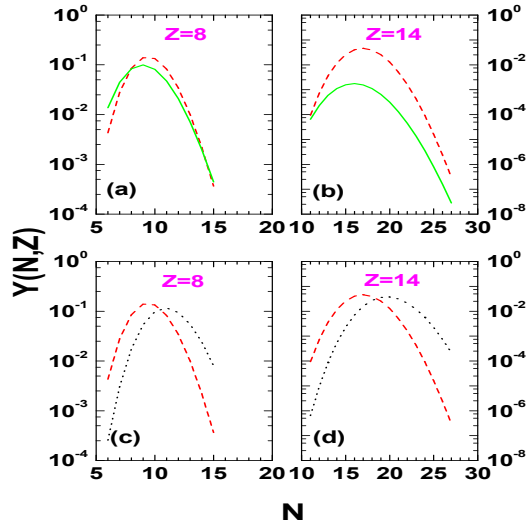


Figure 2. (Color online) Upper Panels: Theoretical isotopic distribution from $A_0 = 168$, $Z_0 = 75$ calculated at $T=5$ MeV (red dashed lines) and 7 MeV (green solid lines). Lower panels: Theoretical isotopic distribution from $A_0 = 168$, $Z_0 = 75$ (red dashed lines) and $A_0 = 186$, $Z_0 = 75$ (black dotted lines) calculated at $T=5$ MeV.

where α and β are isoscaling parameters and C is a normalization constant.

To study the isoscaling in nuclear multifragmentation, we take the dissociating systems having same $Z_1 = Z_2 = 75$ but $A_1 = 168$ and $A_2 = 186$. The ratio R_{21} is plotted in Fig. 3(a) as function of the neutron number for $Z = 6, 8, 10$ and 12 at $T = 5$ MeV. It is seen that the fragments produced by CTM exhibit very well the linear isoscaling behavior. The variation of the isoscaling parameter α with temperature in Fig. 3(b) shows that α gradually decreases with T . α is related to the symmetry energy coefficient C_s used in the liquid-drop formula in eq.(5).

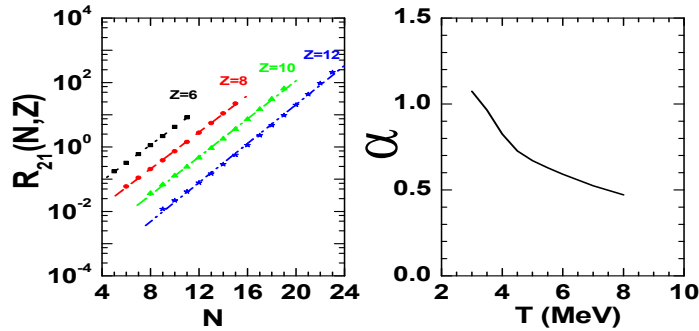


Figure 3. (Color online) Left panel: Ratios (R_{21}) of multiplicities of the fragments (N, Z) where reaction 1 is $A_1 = 168$, $Z_1 = 75$ and reaction 2 is $A_2 = 186$, $Z_2 = 75$. Right panel: Variation of isoscaling parameter (α) with temperature.

5. Extension of CTM to a model for Projectile Fragmentation

Projectile fragmentation is a very useful technique for the production of radioactive ion beam and is also important for astrophysical research. This led to the extension of the canonical thermodynamical model and subsequently development into a model for projectile fragmentation [13–15].

The model for projectile fragmentation reaction consists of three stages: (i) abrasion, (ii) multifragmentation and (iii) evaporation. In heavy ion collision, if the beam energy is high enough, then in the abrasion stage at a particular impact parameter three different regions are formed: (i) projectile spectator or projectile like fragment (PLF) moving in the lab with roughly the velocity of the beam, (ii) participant which suffer direct violent collisions and (iii) target spectator or target like fragment (TLF) which have low velocities in the laboratory. Here we are interested in the fragmentation of the PLF. Using straight-line geometry average number of protons and neutrons present in the projectile spectator at different impact parameters are calculated. The total cross-section of abraded nucleus having Z_s protons and N_s neutrons is [14, 15]

$$\sigma_{a,N_s,Z_s} = \sum_i \sigma_{a,N_s,Z_s,T_i} \quad (7)$$

where the sum is done over all impact parameter intervals and

$$\sigma_{a,N_s,Z_s,T_i} = 2\pi \langle b_i \rangle \Delta b P_{N_s,Z_s}(\langle b_i \rangle) \quad (8)$$

where $P_{N_s,Z_s}(\langle b_i \rangle)$ is the probability of formation of a projectile spectator having Z_s protons and N_s neutrons obtained by using the minimal distribution within the impact parameter interval Δb around $\langle b_i \rangle$ [13].

The multifragmentation stage calculation of each PLF created after abrasion at different impact parameters is done separately by using the Canonical Thermodynamical Model described in section 3. The impact parameter dependence of freeze-out temperature is considered as $T(b) = 7.5 - 4.5(A_s(b)/A_0)$ [15] where $A_s(b)$ is the mass of the projectile spectator created at impact parameter b and A_0 is the mass number of original projectile. So freeze-out temperature of the projectile spectator is independent of the incident beam energy but it depends on the wound in the projectile. This parametrization of temperature profile is obtained by looking at many pieces of data from many nuclear reactions. Almost same PLF size and similar trend of temperature profile is obtained from microscopic calculations [16, 17] also. The freeze-out volume in multifragmentation is $V_f(b) = 3V(b)$ where $V(b)$ is the volume of projectile spectator created at b . Using CTM for an abraded system N_s, Z_s at temperature T_i average population of the composite with neutron number n , proton number z is calculated in the multifragmentation stage. Denoting this by $M_{n,z}^{N_s,Z_s,T_i}$ and summing over all the abraded N_s, Z_s that can yield n, z , the primary cross-section for n, z is

$$\sigma_{n,z}^{pr} = \sum_{N_s,Z_s,T_i} M_{n,z}^{N_s,Z_s,T_i} \sigma_{a,N_s,Z_s,T_i} \quad (9)$$

The excited fragments produced after multifragmentation decay to their stable ground states. Its can γ -decay to shed its energy but may also decay by light particle emission to lower mass nuclei. We include emissions of $n, p, d, t, {}^3\text{He}$ and ${}^4\text{He}$. Particle decay widths are obtained using the Weisskopf's evaporation theory [18]. Fission is also included as a de-excitation channel though for the nuclei of mass < 100 its role will be quite insignificant. Details of the implementation of evaporation model can be found in [19]

6. Results from Projectile Fragmentation Reactions

The projectile fragmentation model is used to calculate the basic observables of projectile fragmentation like the average number of intermediate mass fragments (M_{IMF}), the average size of the largest cluster and their variation with bound charge (Z_{bound}), differential charge distribution, cross-section of neutron rich fragments for different nuclear reactions at intermediate energies with different projectile target combinations.

6.1 M_{IMF} variation with Z_{bound}

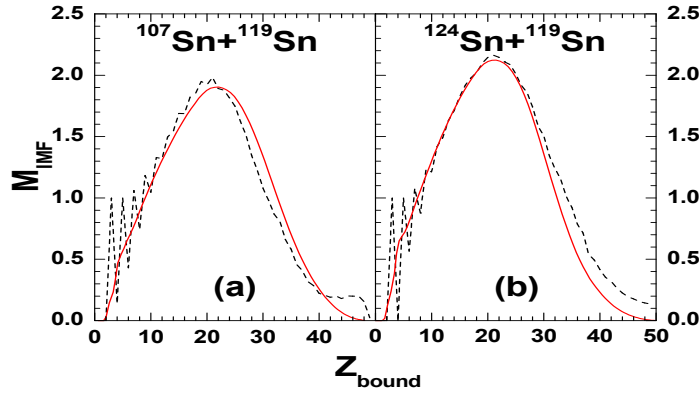


Figure 4. (Color online) Mean multiplicity of intermediate-mass fragments M_{IMF} , as a function of Z_{bound} for (a) ^{107}Sn on ^{119}Sn and (b) ^{124}Sn on ^{119}Sn reaction obtained from projectile fragmentation model (red solid lines). The experimental results are shown by the black dashed lines.

The variation of the average number of intermediate mass fragments M_{IMF} ($3 \leq Z \leq 20$) with Z_{bound} ($=Z_s$ minus charges of all composites with charge $Z = 1$) for ^{107}Sn on ^{119}Sn and ^{124}Sn on ^{119}Sn reactions is shown in Fig.4. The theoretical calculation reproduces the average trend of the experimental data very well. The experiments are done by ALADIN collaboration in GSI at 600A MeV [20]. At small impact parameters, the size of the projectile spectator (also Z_{bound}) is small and the temperature of the dissociating system is very high. Therefore the PLF will break into fragments of small charges (mainly $Z = 1, 2$). Therefore the IMF production is less. But at mid-central collisions PLF's are larger in size and the temperature is smaller compared to the previous case, therefore larger number of IMF's are produced. With further increase of impact parameter, though the PLF size (also Z_{bound}) increases, the temperature is low, hence breaking of dissociating system is very less (large fragment remains) and therefore IMF production is less.

6.2 Differential charge distribution

The differential charge distributions for different intervals of Z_{bound}/Z_0 are calculated by the projectile fragmentation model for ^{119}Sn and ^{124}Sn on ^{119}Sn reactions and compared with experimental data [20]. This is shown in Fig.5. For the sake of clarity the distributions are normalized with different multiplicative factors. At peripheral collisions (i.e. $0.8 \leq Z_{bound}/Z_0 \leq 1.0$) due to small temperature of PLF, it breaks into one large fragment and small number of light fragments, hence the charge distribution shows U type nature.

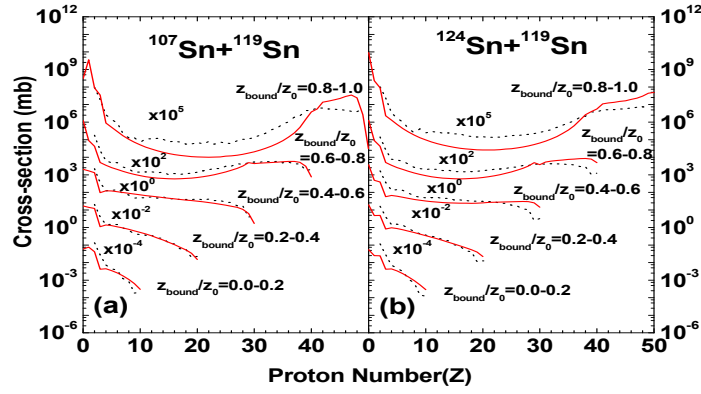


Figure 5. (Color online) Theoretical differential charge cross-section distribution (red solid lines) for (a) ^{107}Sn on ^{119}Sn and (b) ^{124}Sn on ^{119}Sn reaction compared with the experimental data (black dashed lines).

But with the decrease of impact parameter the temperature increases, the PLF breaks into larger number of fragments and the charge distributions become steeper. The features of the data are nicely reproduced by the model.

6.3 Size of largest cluster and its variation with Z_{bound}

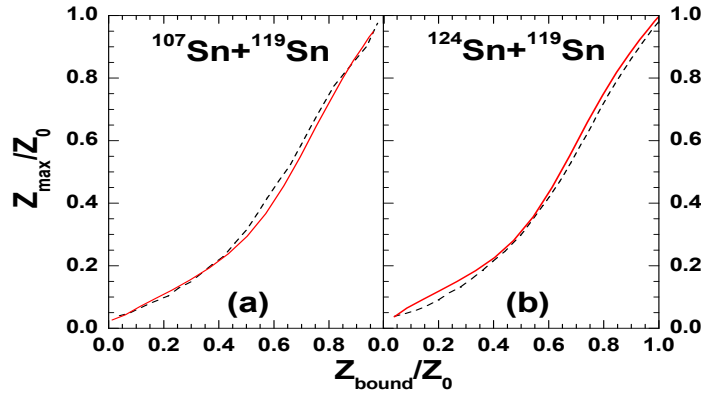


Figure 6. (Color online) Z_{max}/Z_0 as a function of Z_{bound}/Z_0 for (a) ^{107}Sn on ^{119}Sn and (b) ^{124}Sn on ^{119}Sn reaction obtained from projectile fragmentation model (red solid lines). The experimental results are shown by the black dashed lines.

Average size of the largest cluster produced at different Z_{bound} values is calculated in the framework of projectile fragmentation model for ^{119}Sn and ^{124}Sn on ^{119}Sn reactions. In Fig.6 the variation of Z_{max}/Z_0 (Z_{max} is the average number of proton content in the largest cluster) with Z_{bound}/Z_0 obtained from theoretical calculation and experimental result are shown. Very nice agreement with experimental data is observed.

6.4 Cross-section and binding energy of neutron rich nuclei

Projectile fragmentation cross-sections of many neutron-rich isotopes have been measured experimentally from the ^{48}Ca and ^{64}Ni beams at 140 MeV per nucleon on ^9Be and ^{181}Ta targets [21]. Our theoretical model reproduces the cross-sections of projectile fragmentation experiments very well [13–15]. A remarkable feature is the co-relation between the measured fragment cross-section (σ) and the binding energy per nucleon (B/A). This observation has prompted attempts of parametrization of cross-sections [22–24]. One very successful parametrization is

$$\sigma = C \exp\left[\frac{B}{A} \frac{1}{\tau}\right] \quad (10)$$

Here τ is a fitting parameter. In this parametrization we have not considered the pairing

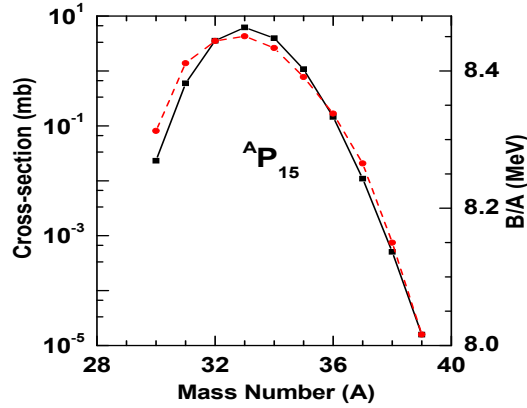


Figure 7. Fragment cross-section (circles joined by red dotted line) for ^{64}Ni on ^9Be reaction and binding energy per nucleon (squares joined by black solid line) plotted as a mass number for $Z = 15$ isotopes.

energy contribution in nuclear binding energy. Here we have calculated production cross-sections $Z = 15$ isotopes for ^{64}Ni on ^9Be reaction from projectile fragmentation model and plotted in log scale in Fig.-7 (circles joined by red dotted line). The variation of the theoretical binding energy per nucleon for same isotopes of $Z = 15$ in linear scale is also shown in the same figure (squares joined by black solid line). The similar trend of the cross-section curve (in log scale) and binding energy curve (in linear scale) confirms the validity of above parametrization from our model. By this method we can interpolate (or extrapolate) the cross-section of an isotope if the binding energy is known. We can also estimate the binding energy of an isotope by measuring its cross-section experimentally..

7. Application of Nuclear Multifragmentation

Nuclear multifragmentation is very useful for studying nuclear liquid gas phase transition and for investigation of nuclear matter at sub-saturation densities. Projectile fragmentation is very useful technique for production of radioactive ion beam and is useful for nuclear structure studies as well as for astrophysical research. Nuclear multifragmentation can be used for spallation reaction (nuclear power production), nuclear waste management (environment protection), proton and ion therapy (medical applications), radiation

protection of space missions (space research) etc. Thus nuclear multifragmentation is an important tool in basic research as well as in a wide variety of other applications.

8. Summary

The study of nuclear multifragmentation is an important area of research in intermediate energy heavy-ion collisions. The canonical thermodynamical model which is based on analytic evaluation of the partition function has been used to calculate different observables characterizing the multifragmentation reaction and some simple results are displayed. This simple analytical model is extended to develop a model for projectile fragmentation which is important for the study of exotic nuclei as well as for astrophysical research. A few typical observables like average multiplicity of intermediate mass fragments, differential charge distribution, cross-section of neutron rich nuclei, size of the largest cluster and its variation with Z_{bound} are calculated using this model and their good agreement with experimental data confirms the justification of the assumptions made in the model. Apart from basic research, the disintegration of the excited nuclei into many pieces also finds its application in a wide variety of other fields.

References

- [1] G. F. Bertsch and S. Das Gupta, Phys. Rep **160**, 189 (1988).
- [2] A. Ono and H. Horiuchi, Prog. Part. Nucl. Phys **53**, 501 (2004).
- [3] C. Hartnack et al., Eur. phys. J. **A1** 151 (1998)
- [4] C. B. Das, S. Das Gupta et al., Phys. Rep **406**, 1 (2005).
- [5] J. P. Bondorf et al., Phys. Rep. **257**, 133 (1995).
- [6] D. H. Gross, Phys. Rep **279**, 119 (1997).
- [7] J. Randrup and S. E. Koonin, Nucl. Phys. **A 471**, 355c (1987).
- [8] K.C. Chase and A. Z. Mekjian, Phys. Rev. C **52**, R2339 (1995).
- [9] S. Mallik and G. Chaudhuri, Phys. Lett. **B 718** (2012) 189.
- [10] G. Chaudhuri, F. Gulminelli and S. Mallik, Phys. Lett. **B 724** (2013) 115.
- [11] M. B. Tsang et al., Phys. Rev. Lett. **86**, 716 (2000).
- [12] G. Chaudhuri, S. Das Gupta and M. Mocko, Nucl. Phys. **A 813**, 293 (2008).
- [13] S. Mallik, G. Chaudhuri and S. Das Gupta, Phys. Rev. C **83**, 044612 (2011).
- [14] S. Mallik, G. Chaudhuri and S. Das Gupta, Phys. Rev. C **84**, 054612 (2011).
- [15] G. Chaudhuri, S. Mallik and S. Das Gupta, Jour. of Phys. Conf. Series **420**, 012098 (2013).
- [16] S. Das Gupta, S. Mallik and G. Chaudhuri, arxiv1305.1140, Phys. Lett. **B** (Article in Press).
- [17] S. Mallik, S. Das Gupta and G. Chaudhuri, arxiv1309.4064.
- [18] V. Weisskopf, Phys. Rev. **52**, 295 (1937).
- [19] G. Chaudhuri and S. Mallik, Nucl. Phys. **A 849**, 190 (2011).
- [20] R. Ogul et al., Phys. Rev C **83**, 024608 (2011).
- [21] M. Mocko et al., Phys. Rev C **74**, 054612 (2006).
- [22] M. Mocko et al., Eur. phys. Lett. **79** (2007) 12001.
- [23] M. B. Tsang et al., Phys. Rev C **76**, 041302 (R) (2007).
- [24] G. Chaudhuri et al., Phys. Rev C **76**, 067601 (2007).